A density-functional theory study of the interaction of N_2O with Rh(110)

Anton Kokalj[a)]
Jožef Stefan Institute, 1000 Ljubljana, Slovenia

Tatsuo Matsushima
Catalysis Research Center, Hokkaido University, Sapporo 060-0811, Japan

(Received 29 June 2004; accepted 18 October 2004; published online 3 January 2005)

The adsorption of nitrous oxide, N_2O, on a Rh(110) surface has been characterized by using density-functional theory. N_2O was found to bind to the surface in two alternative forms. The first, less stable form is tilted with the terminal N atom attached to the surface, while the second, more stable form lies horizontally on the surface. Adsorption on the on-top site is more stable than that on the bridge site. The tilted form remains linear on adsorption, while the horizontal form is bent, with the terminal-nitrogen and oxygen atoms pointing towards the surface. At lower adsorbate coverage, $\Theta \lesssim 1/4$ ML (ML—monolayer), the adsorption of a few horizontal N_2O configurations is dissociative, i.e., $N_2O \rightarrow N_2(a) + O(a)$. The N_2O-surface interaction is discussed in terms of the electronic structure analysis. © *2005 American Institute of Physics.* [DOI: 10.1063/1.1829652]

I. INTRODUCTION

Nitrous oxide, N_2O, is an intermediate in the removal of NO_x on automobile three-way catalysts. Furthermore, N_2O itself is harmful and yields a remarkable greenhouse effect. Therefore its decomposition on noble metals has attracted much attention, because these metals are good catalysts and N_2O is the main byproduct in this process.[1] In particular, much attention have been given to the decomposition of N_2O on rhodium surfaces, because rhodium is one among the best catalysts for removing nitrogen oxides.[2] Despite the importance of this system, the interaction of N_2O with rhodium surfaces is not yet well understood. Peculiar inclined N_2 desorption observed recently on some fcc(110) surfaces[3–12] is expected to provide further insight. On a Rh(110) surface, the nitrogen molecules produced during the thermal dissociation of N_2O were detected to desorb in inclined bidirectional lobes in a plane along the [001] direction.[10,12] The collimation angle was about 70°, which is larger than 43°–50° found on Pd(110).[7] Recent report of N_2O adsorption on a clean Rh(110) showed significant dissociation to $N_2(a)$ and $O(a)$ at temperatures around 60 K [where $X(a)$ refer to adsorbed X species, this notation will be used hereafter] at small N_2O exposures,[13] indicating that the dissociation barrier is rather small.

Computational studies of N_2O adsorption on transition metal surfaces are very scarce.[14–17] Instead, several authors have reported on the interaction and decomposition of N_2O with transition metal atoms[18–20] or small clusters.[21] Burch *et al.*[22] studied the formation of N_2O via the NO+N reaction on Pt(111) surface using density-functional theory (DFT), but the adsorption of N_2O was not discussed. Bogicevic and Hass[23] performed DFT study of NO pairing and transformation to N_2O on Cu(111) and Pd(111). They briefly mentioned that N_2O is preferentially adsorbed on the on-top site, but geometry of the adsorbed N_2O was not discussed. To the best of our knowledge, the interaction of N_2O with Rh surfaces (or atoms) has not yet been studied by computational first-principle methods. For this reason we have undertaken a DFT study of N_2O adsorption on Rh(110) surface. Since very little is known about the nature of the N_2O chemical bonding with transition metal surfaces, we discuss in this work to some depth the electronic factors that govern the adsorption phenomenon.

The structure of the adsorbed N_2O is an important ingredient to provide an explanation of the mechanism of the above-mentioned peculiar N_2 desorption. Moreover, the structure of $N_2O(a)$ immediately before dissociation can be studied only by means of theoretical calculations. In our previous contributions[14,15] we studied the adsorption structures of N_2O on Pd(110). In this paper we report on a detailed first-principle density-functional study of the geometry and orientation of $N_2O(a)$ on Rh(110) at coverages ranging from 1/6 to 1 monolayer (ML).

II. COMPUTATIONAL METHOD

All calculations were performed with the DFT using the generalized gradient approximation (GGA) of Perdew–Burke–Ernzerhof (PBE).[24] Nuclei and core electrons were described by ultrasoft pseudopotentials.[25,26] The Kohn–Sham orbitals were expanded in a plane-wave basis set with a kinetic energy cutoff of 27.5 Ry (220 Ry for the charge-density cutoff). Brillouin zone (BZ) integrations have been performed with the Gaussian-spreading special-point technique[27,28] with a smearing parameter of 0.03 Ry. Calculations have been done using the PWSCF package,[29] while molecular graphics were generated by the XCRYSDEN (Refs. 30 and 31) graphical package.

The perfect Rh(110) surface was modeled by periodically repeated slabs consisting of five (110) layers and vacuum region of 12.5 Å. N_2O molecules were adsorbed on one side of the slab (by using the stated vacuum thickness

a)Fax: +386-1-477-3811. Electronic mail: Tone.Kokalj@ijs.si; URL http://www-k3.ijs.si/kokalj/

TABLE I. Surface energies σ, work functions ϕ, relaxations of the first layer Δd_{12}, second layer Δd_{23} of a Rh(110) surface, and N_{layers} number of layers in the slab.

	N_{layers}	σ (eV/atom)	σ (eV/Å^2)	ϕ (eV)	Δd_{12} (%)	Δd_{23} (%)
Present work	5	1.55[a]	0.146[a]	4.62	−12.0	+3.6
	7	1.59[a]	0.150[a]	4.72	−10.1	+3.5
	9	1.58[a]	0.149[a]	4.57	−9.4	+1.1
	11			4.53	−10.3	+2.1
	7,9,11	1.60[b]	0.150[b]			
GGA FP-LAPW[c]	7	1.43	0.138	4.59	−9.2	+2.1
Experiment		1.69[d]	0.17[d]	4.98[e]	-6.9 ± 1.0[f]	$+1.9\pm1.0$[f]

[a]Surface energies estimated by equation $\sigma=1/2\{E_{\text{slab}}(N)-N/2[E_{\text{slab}}(11)-E_{\text{slab}}(9)]\}$.
[b]Surface energy calculated by fitting the equation $E_{\text{slab}}(N)=2\sigma+NE_{\text{bulk}}$.
[c]Reference 38.
[d]Data from Ref. 39, σ corresponds to an "average" high-index surface.
[e]Data from Ref. 34.
[f]Data from Ref. 35.

the N_2O molecules are more than 8 Å away from the adjacent slab). N_2O adsorption was modeled at 1, 1/2, 1/3, 1/4, and 1/6 ML coverages and (2×1), (3×1), (4×1), (2×2), (3×2), c(2×2), and c(2×4) supercells were used. The BZ integrations were performed with a 5×5, and 3×3 uniform shifted k mesh[32] for the c(2×2), and c(2×4) primitive supercells, respectively, while for (2×1), (3×1), (4×1), (2×2), and (3×2) supercells the 4×6, 3×6, 2×6, 4×3, and 3×3 uniform shifted k meshes were used, respectively. The calculated bulk lattice parameter was used as the in-plane lattice spacing. The spacing of the bottom three layers of the slab was fixed at the bulk interplane spacing, whereas the geometries of the top two layers and N_2O molecule were fully optimized using the Broyden-Fletcher-Goldfarb-Shanno algorithm[33] with analytically calculated forces according to Hellmann-Feynmann theorem. In all the optimized systems the forces acting on the atoms, which were allowed to relax are below 10^{-3} Ry/a_0.

The binding energy E_b of adsorbed N_2O was calculated as $E_b=(E_{\text{Rh(110)}}+E_{\text{N}_2\text{O}})-E_{\text{N}_2\text{O/Rh(110)}}$, where $E_{\text{Rh(110)}}$, $E_{\text{N}_2\text{O}}$, and $E_{\text{N}_2\text{O/Rh(110)}}$ are the potential energies of the pure substrate, the isolated N_2O molecule, and the N_2O/substrate adsorption system, respectively. With this definition, positive binding energies indicate stable adsorption.

III. RESULTS

A. Isolated constituents: Bulk Rh, Rh(110) surface, and the N_2O(g)

The experimental lattice parameter of bulk rhodium is 3.80 Å,[34] whereas our GGA calculations yield 3.87 Å—an overestimation of 2%. This agrees with the results obtained by the other GGA pseudopotential calculations, 3.85 Å (Ref. 36) and 3.87 Å.[37] The lattice parameter predicted by GGA full-potential linearized augmented-plane-wave (FP-LAPW) method is 3.83 Å.[38] Our GGA calculated bulk modulus is 250 GPa, while experimental value is 269 GPa.[40] This agrees with the results obtained by the FP-LAPW method, 259 GPa,[38] and other pseudopotential calculations, 244 GPa (Ref. 36) and 251 GPa.[37]

The properties of the clean Rh(110) surface have been calculated using 5-, 7-, 9- and 11-layer slabs with a 1×1 surface geometry and the BZ integrations were performed by 8×6 uniform shifted k-mesh. All the layers have been relaxed symmetrically for these calculations. The surface energy σ was estimated (i) by applying the Boettgerlike equation,[41] $\sigma=1/2\{E_{\text{slab}}(N)-N/2[E_{\text{slab}}(11)-E_{\text{slab}}(9)]\}$, and (ii) by fitting the slab potential energies $E_{\text{slab}}(N)$ for $N=7$, 9, 11 to the equation $E_{\text{slab}}(N)=2\sigma+NE_{\text{bulk}}$, where N and E_{bulk} stand for number of layers in the slab and bulk energy, respectively. The work function ϕ was calculated as the difference between the average electrostatic potential in the vacuum and the Fermi level. The calculated properties of the clean Rh(110) surface are reported in Table I. Our GGA calculations yield $\sigma=1.60$ eV/atom$=0.15$ eV/Å^2 and $\phi=4.6\pm0.1$ eV. The relaxations of the first Δd_{12} and second Δd_{23} layers are $-10\pm1\%$ and $+2\pm1\%$, respectively, while experimental values are $\Delta d_{12}=-6.9\pm1.0\%$ and $\Delta d_{23}=+1.9\pm1.0\%$.

The N_2O molecule is an anomalous member of AB_2 family of triatomic molecules, as it has asymmetric arrangement of its nuclei, i.e., $A-A-B$. For the ease of discussion we define the symbols N_t and N_c which stand for the terminal- and the central-nitrogen atoms, respectively. For the N_2O molecule in the gas phase our calculations predict a linear geometry with a nitrogen-nitrogen distance (d_{NN}) of 1.142 Å, and a nitrogen-oxygen distance (d_{NO}) of 1.210 Å, which agree with the B3LYP (Becke-3 Lee-Yang-Parr) calculated distances (1.134 and 1.193 Å, respectively).[42] The experimental values are 1.128 Å for d_{NN} and 1.184 Å for the d_{NO} distance.[34]

B. Adsorption structures and energies

Several possible configurations of molecular adsorption on the Rh(110) surface were examined in order to determine the orientation and site preference of the N_2O molecule. In particular, the adsorption was modeled by attaching the N_2O molecule either with the terminal nitrogen (hereafter labeled as N_t bonded), the central nitrogen (N_c bonded), or the terminal oxygen atom (O bonded) to the surface, and by placing the molecule horizontally on the surface so that its terminal

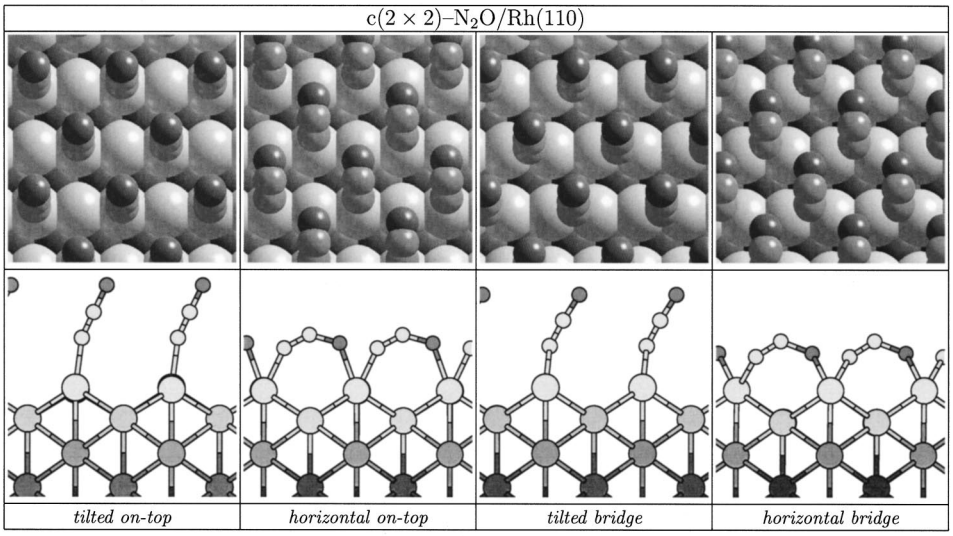

FIG. 1. Top and side views of optimized N_2O/Rh(110) structures for c(2×2) supercells representing 1/2 ML coverage. Larger balls are Rh atoms, while smaller gray (dark-gray) balls are N (O) atoms.

nitrogen and oxygen atoms are interacting with the substrate atoms (hereafter designated as *horizontal* form). The horizontal forms will be labeled as $site_1(N_t)$-$site_2(O)$, meaning that the N_t atom is pointing toward the $site_1$ site and O atom toward the $site_2$. The N_t and O atoms can point either to the same type of site, i.e., on-top(N_t)–on-top(O) or bridge(N_t)–bridge(O), or to different type of site, i.e., on-top(N_t)–bridge(O) or bridge(N_t)–on-top(O). For brevity, the on-top(N_t)–on-top(O) or bridge(N_t)–bridge(O) forms will be referred shortly as on-top and bridge, respectively.

1. Molecular and dissociative adsorption of N_2O

Calculations indicate that the $N_2O(a)$ binds to the surface in two forms. The first, less stable form is linear and tilted with the terminal N atom attached to the surface. The d_{NN} and d_{NO} distances are almost unchanged on adsorption. Precise estimation of the tilt angle is difficult due to the flatness of the potential energy surface. The second, more stable form lies horizontally on the surface and is bent, with the terminal nitrogen and oxygen atoms pointing toward the surface. The d_{NN} and d_{NO} distances are longer than in the tilted structures. The optimized tilted and horizontal $N_2O(a)$ structures at 1/2 ML coverage are shown in Fig. 1. Here, the horizontal molecular structures are oriented along the [001] direction. The binding energies E_b and structural parameters of N_2O adsorbed on the on-top and bridge sites for the two forms are listed in Table II. These adsorbed structures are analogous to those found previously on a Pd(110) surface.[15] However, on Rh(110) the horizontal form is more stable by 0.2–0.3 eV than the tilted one, while their stabilities on Pd(110) are very similar, the E_b being ~0.4 eV. Hence, N_2O binds more strongly to the Rh(110) surface, which is not surprising as Rh has less occupied *d* bands. Adsorption on the on-top sites is energetically favorable on both surfaces and the bridge configurations are less stable.

An interesting result is that at lower adsorbate coverage $\Theta \lesssim 1/4$ ML the adsorption of horizontal bridge form is dissociative, namely, the N_2O decomposes to $N_2(a)+O(a)$ during the geometry optimization calculation, presumably due to the absence of a dissociation barrier, leading to adsorbed nitrogen molecule and $O(a)$.

The adsorption of horizontal $N_2O(a)$ was modeled oriented either along the [001], [110], or [112] direction. Binding energies and structural parameters of various horizontal forms are reported in Table III, while top and side views of optimized structures are shown in Fig. 2. The $N_2O(a)$ oriented along [001] was predicted to be more stable than that oriented along the [110] direction, the E_b being

TABLE II. Calculated binding energies E_b and structural parameters of the tilted and horizontal $N_2O(a)$ moieties oriented in the [001] direction. The labels d_{RhN}, d_{NN}, d_{NO}, and d_{RhO} stand for the distances between the corresponding atoms.

Site	Moiety	Super cell	Coverage (ML)	E_b (eV)	d_{RhN} (Å)	d_{NN} (Å)	d_{NO} (Å)	d_{RhO} (Å)
On-top	Tilted	c(2×2)	1/2	0.53	2.03	1.15	1.22	
		c(2×4)	1/4	0.53	2.04	1.15	1.22	
	Horizontal	c(2×2)	1/2	0.71	1.98	1.19	1.30	2.11
		c(2×4)	1/4	0.82	1.96	1.20	1.33	2.08
Bridge	Tilted	c(2×2)	1/2	0.25	2.23	1.16	1.22	
		c(2×4)	1/4	0.24	2.22	1.16	1.22	
	Horizontal	c(2×2)	1/2	0.42	2.13	1.22	1.39	2.20
		c(2×4)	1/4	Dissociates to $N_2(a)+O(a)$				
	$N_2O(g)$					1.14	1.21	

TABLE III. Calculated binding energies and structural parameters of the various horizontal $N_2O(a)$ forms, oriented in the [001], [1$\bar{1}$0], and [11$\bar{2}$] directions, or placed on the surface ''asymmetrically''—the terminal N_t and O atoms pointing toward the top (bridge) and bridge (top) site, respectively. The ''asymmetric'' forms are labeled as bridge(N)$_t$–on-top(O) and on-top(O)—bridge(N_t). Other labels have the same meaning as in Table II.

Supercell	Coverage (ML)	Moiety	Orientation	E_b (eV)	d_{RhN} (Å)	d_{NN} (Å)	d_{NO} (Å)	d_{RhO} (Å)
c(2×4)	1/4	On-top horizontal	[00$\bar{1}$]	0.82	1.96	1.20	1.33	2.08
		On-top horizontal	[11$\bar{2}$]	Dissociates to $N_2(a)+O(a)$				
		Bridge(N_t)–on-top(O)	Asymmetric	0.67	2.03/2.15	1.24	1.32	2.11
		On-top(N_t)–bridge(O)	Asymmetric	Dissociates to $N_2(a)+O(a)$				
(3×1)	1/3	On-top horizontal	[1$\bar{1}$0]	0.60	1.97	1.20	1.36	2.05
(3×2)	1/6	On-top horizontal	[1$\bar{1}$0]	0.65	1.97	1.21	1.37	2.05

0.82 and 0.65 eV, respectively, while the adsorption of [11$\bar{2}$]-oriented molecule is dissociative, namely, the geometry optimization calculation leads to dissociated $N_2O(a)$—presumably due to the absence of a dissociation barrier or at least very small and narrow barrier—resulting to $N_2(a)$ and $O(a)$. The molecule was also placed on the surface ''horizontally-asymmetric,'' i.e., it bridged atomic troughs of the substrate that are extending in the [1$\bar{1}$0] direction and one of the terminal atoms (N_t or O) of the molecule was pointing toward the on-top site, while the other toward the bridge site, i.e., on-top(N_t)–bridge(O) and bridge(N_t)–on-top(O) structures. The calculated E_b of bridge(N_t)–on-top(O) structure is 0.67 eV. This structure is therefore less stable than the horizontal on-top structure oriented in the [001] direction. Note that the bend of bridge(N_t)–on-top(O) structure is somewhat peculiar as the molecule is not bent only toward the surface, but also laterally (see Fig. 2). The adsorption of the other ''asymmetric'' structure, on-top(N_t)–bridge(O), is predicted to be dissociative—a prediction similar to that for the [11$\bar{2}$]-oriented molecule.

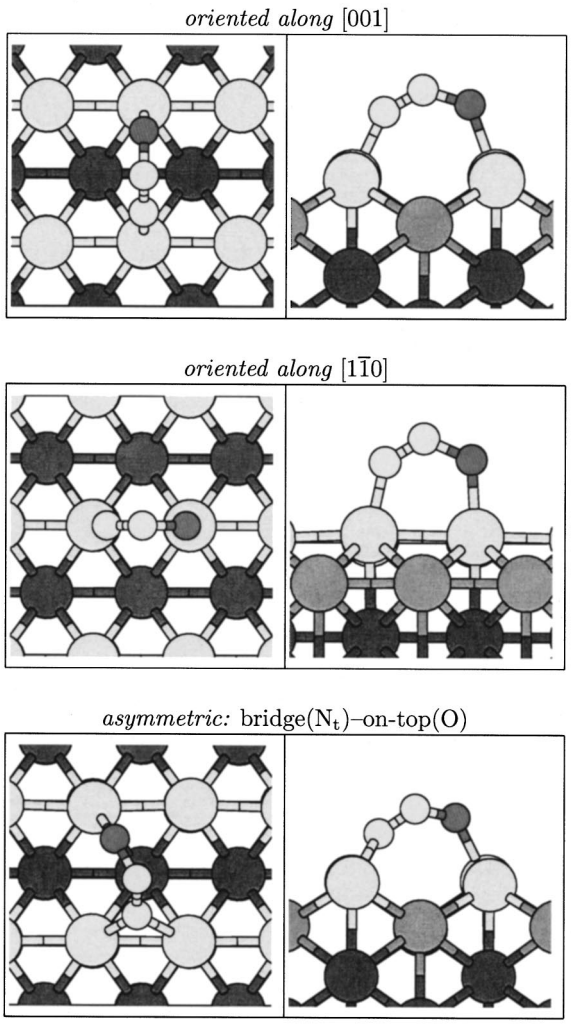

FIG. 2. Top and side views of optimized horizontal $N_2O(a)$ structures oriented along the [001] and [1$\bar{1}$0] directions and asymmetric bridge (N_t)–on-top(O) form.

2. "In-phase" versus "out-of-phase" tilt

The $N_2O(a)$ molecules can be considered tilted either in the same direction, i.e., in-phase tilt, or tilted such that adjacent molecules point in opposite direction, i.e., out-of-phase tilt. As the coverage of the admolecules increases the molecule-molecule lateral distances are becoming smaller, and the lateral molecule-molecule interactions more important. The out-of-phase tilt provide a packing where the adjacent molecules are avoiding each other better than the in-phase tilted molecules (see Fig. 3). The calculations indicate that at full monolayer coverage, the out-of-phase tilting configuration is more stable than the in-phase one, the E_b being

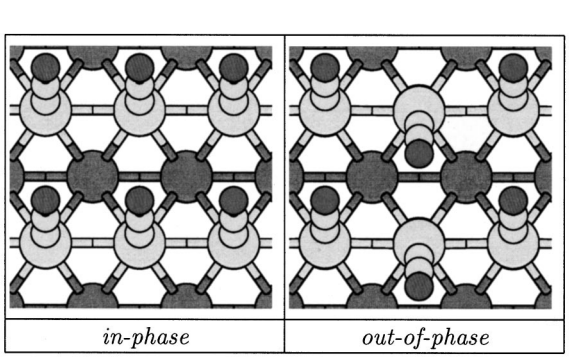

FIG. 3. Top-view of the ''in-phase'' and ''out-of-phase'' tilting $N_2O(a)$ configurations at 1 ML coverage.

TABLE IV. "Out-of-phase" vs "in-phase" on-top tilted $N_2O(a)$: calculated binding energies and structural parameters. Full monolayer coverage $\Theta=1$ ML has been modeled by placing two molecules in a (2×1) supercell, while for $\Theta=1/2$ ML two molecules were placed inside the (4×1) supercell. The labels have the same meaning as in Table II.

Site and moiety	Supercell	Coverage (ML)	Tilt	E_b (eV)	d_{RhN} (Å)	d_{NN} (Å)	d_{NO} (Å)
On-top tilted	(2×1)	1	In-phase	0.23	2.04	1.15	1.22
			Out-of-phase	0.39	2.03	1.15	1.22
	(4×1)	1/2	In-phase	0.54	2.04	1.15	1.22
			Out-of-phase	0.54	2.04	1.15	1.22

0.39 and 0.23 eV, respectively. However, already at 1/2 ML coverage the difference in E_b between the two tilting configurations become insignificant. Table IV summarizes the binding energies and structural parameters of in-phase and out-of-phase tilted configurations at 1/2 and 1 ML coverage.

3. Less stable and unstable $N_2O(a)$ forms

Calculations indicate that the N_2O cannot adsorb on the Rh(110) surface with the central-nitrogen atom—such an interaction is predicted to be repulsive.

The calculations also predicted a highly tilted N_2O form adsorbed to on-top site and attached to the surface via the oxygen atom (see Fig. 4), with very small binding energy of 0.15 eV and large oxygen-surface distance of 2.5 Å [note that for the on-top tilted $N_2O(a)$ adsorbed via the N_t atom, the N_t-surface distance is only 2.03 Å]. Such a weakly oxygen bonded and highly tilted N_2O form is also predicted on Pd(110).[43] The E_b for the highly tilted O-bonded molecule adsorbed on the bridge site is similar, 0.12 eV. Results for the O-bonded $N_2O(a)$ forms are summarized in Table V. These tiny binding energies for the O-bonded molecules are comparable with energies given by dispersion forces, moreover, the molecule-surface distances are quite large. At such large distances the dispersion forces are expected to be important, and hence the DFT predictions less reliable. Whether these GGA predicted energies are meaningful is questionable, because GGA is not able to describe the dispersion interactions. In our previous study,[16] we calculated the interaction between N_2O and a single Pd atom—the N_2O was bonded with the oxygen atom to palladium. The current DFT implementation predicted the binding energy of 0.28 eV, while the binding energy predicted by the second-order Møller-Plesset perturbation theory[44] was virtually zero.

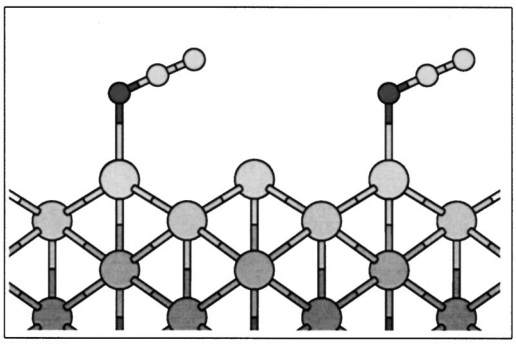

FIG. 4. Side view of the optimized highly tilted $N_2O(a)$ structure adsorbed with O atom to the on-top surface site.

IV. DISCUSSION

A. Stable adsorption and dissociation of N_2O

Calculations predict the attractive adsorbate-substrate interaction when the molecule is adsorbed in a tilted configuration bonded to the surface with the N_t atom, or lying horizontally on the surface. At lower adsorbate coverage $\Theta\lesssim1/4$ ML the adsorption of some horizontal N_2O configurations is predicted to be dissociative, i.e., $N_2O\rightarrow N_2(a)+O(a)$.

The geometry of the tilted $N_2O(a)$ is linear and intramolecular distances are almost unchanged on adsorption. In the case of horizontal $N_2O(a)$, the geometry is not linear but bent, with the N_t and O atoms pointing toward the surface. The d_{NN} and d_{NO} distances are greater than in the tilted structures—an indication of larger charge backdonation into the antibonding 3π molecular orbital. This charge backdonation is evidenced in the projected density of states[45] (PDOS) plots shown in Fig. 6, and by integrated local density of states[46] (ILDOS) plots of Fig. 8. This issue will be described in more detail below (see Sec. IV B).

The geometry of adsorbed N_2O on transition metal surfaces has not been widely studied experimentally (see recent review of Zeigarnik[47] or Matsushima[48]). It has been proposed that N_2O adsorbs via the terminal nitrogen atom in an inclined[49–52] or upright[49,53,54] form. The inclined form was proposed on the basis of vibrational spectroscopy work on Ru(001) (Ref. 49) and Pt(111),[50] NEXAFS (near edge x-ray absorption fine structure spectroscopy) analysis on Ni(111) (Ref. 51) and Cu(100),[52] and also use of the kinetic isotope effects approach to polycrystalline Cu.[55] However, the angle of tilt is still unclear from experimental work, because there

TABLE V. Highly tilted $N_2O(a)$ forms adsorbed with the oxygen atoms to the surface, i.e., O-bonded forms: calculated binding energies and structural parameters. The labels have the same meaning as in Table II.

Site	Moiety	Supercell	Coverage (ML)	E_b (eV)	d_{RhO} (Å)	d_{NN} (Å)	d_{NO} (Å)
On-top	Tilted O-bonded	$c(2\times2)$	1/2	0.15	2.5	1.14	1.22
		$c(2\times4)$	1/4	0.15	2.5	1.14	1.22
Bridge	Tilted O-bonded	$c(2\times2)$	1/2	0.12	3.15	1.14	1.21

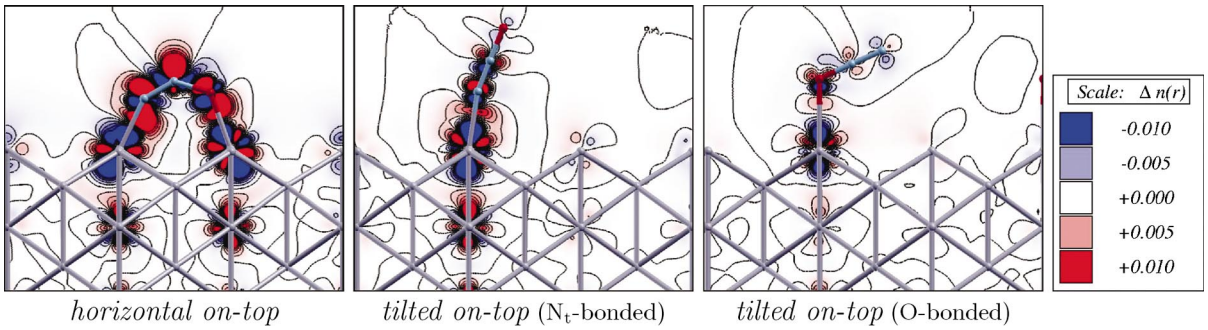

FIG. 5. (Color) Charge density difference $\Delta n(\mathbf{r}) = n_{N_2O/Sub}(\mathbf{r}) - [n_{Sub}(\mathbf{r}) - n_{N_2O}(\mathbf{r})]$ for the horizontal on-top, and N_t and O bonded tilted on-top $c(2\times4)-N_2O/Rh(110)$ structures. The contours are drawn in linear scale from $-0.01e/a_0^3$ to $0.01e/a_0^3$, with the increment of $0.002e/a_0^3$. The charge flows from blue to red regions.

are difficulties in NEXAFS analysis which would provide the most reliable orientation (see discussion section in our previous study, Ref. 15).

Very recent NEXAFS measurements of N_2O on Pd(110) at around 60 K suggest that a majority of N_2O is in a horizontal form oriented along the [001] direction and a minor amount is standing,[56] while no anisotropy was found in NEXAFS spectra on Rh(110), i.e., neither [001] oriented, nor $[1\bar{1}0]$ oriented N_2O nor the standing form was excluded.[13] The $N_2O(a)$ forms as predicted by the DFT-GGA calculations for Pd(110) (Ref. 15) seem to be in agreement with these NEXAFS measurements, while the analogous $N_2O(a)$ forms on Rh(110) predicted in this work are contradicting the NEXAFS results, namely, calculations indicate the [001] orientation of the horizontal form is more stable than the standing and $[1\bar{1}0]$-oriented horizontal form.

In order to reconcile the above mismatch between the NEXAFS results and DFT-GGA predictions of $N_2O/Rh(110)$ we pass the discussion to the molecular versus dissociative adsorption of N_2O. In recent $N_2O/Rh(110)$ experiments[10–13,57] a significant amount of dissociated N_2O, i.e., $N_2(a)+O(a)$, was observed already at a temperature below 100 K. The NEXAFS measurements[13] indicate the dissociative N_2O adsorption takes place already at temperature around 60 K. These findings suggest that for some $N_2O(a)$ configurations the dissociation barrier must be very low. The DFT-GGA calculations indicate that indeed some forms of horizontal $N_2O(a)$ dissociate readily (i.e., during the geometry optimization the N_2O is decomposed to $N_2(a)$ and $O(a)$ presumably due to the absence of a dissociation barrier or at least very narrow and small dissociation barrier). A similar dissociative behavior of N_2O was also predicted by Orita and Itoh—using DFT-GGA calculations—on step edge sites of Ni(755) surface.[17] Our preliminary constrained-optimization calculations, where the N–O distance was stepwise increased and all the other degrees of freedom were optimized, indicate that the dissociation barrier for the most stable [001]-oriented horizontal $N_2O(a)$ form is very small. At 1/2 ML coverage it is ~0.15 eV, and is expected to be even smaller at lower coverage. This might indicate that the [001]-oriented horizontal $N_2O(a)$ is prone to dissociate already at temperature at which the NEXAFS spectra were recorded. The most remarkable difference in NEXAFS measurements between Pd(110) and Rh(110) is in the amount of coadsorbed oxygen. At surface temperature of 60 K, no $O(a)$ was detected on Pd(110), while about 20% of incident N_2O released $O(a)$ on Rh(110).[57] At present, it is not known how this $O(a)$ affects the orientation of $N_2O(a)$.

B. Electronic structure of adsorbed N_2O

Since very little is known about the nature of the N_2O chemical bond with transition metal surfaces, the electronic factors that govern the adsorption phenomenon are discussed below.

We start the discussion of the electronic structure by observation that the oxygen-surface distance of the horizontal $N_2O(a)$ form (2.1 Å for the on-top structure) is substantially shorter than 2.5 Å predicted for the O-bonded on-top tilted structure. Such short oxygen-surface distance is a clear indication that the horizontally adsorbed molecules also interact with the surface through the oxygen atom. This conclusion is supported by the accumulation of the charge in the Rh–O bonding region—as seen from the charge density difference $\Delta n(\mathbf{r}) = n_{N_2O/Sub}(\mathbf{r}) - [n_{Sub}(\mathbf{r}) + n_{N_2O}(\mathbf{r})]$ displayed in Fig. 5—and is further evidenced by the ILDOS plots in Fig. 8. The $n_{N_2O/Sub}(\mathbf{r})$, $n_{Sub}(\mathbf{r})$, and $n_{N_2O}(\mathbf{r})$ are the electron charge density distributions of the N_2O-on-substrate, clean substrate, and N_2O, respectively. Compare, for example, charge accumulated between oxygen and surface for the horizontal and O-bonded tilted structures. Clearly, as seen from Fig. 5, such accumulation is substantial only for the former structure. The $\Delta n(\mathbf{r})$ plots in Fig. 5 show that the redistribution of the charge on adsorption is larger for the horizontal form than for the N_t-bonded tilted form. The charge redistribution of the O-bonded tilted form is the smallest, thus being consistent with a very tiny predicted adsorption energy.

Now we describe in more detail the PDOS plots of Fig. 6, where PDOS is projected to N_2O molecule and to the surface Rh atoms that interact with the N_2O molecule for the tilted on-top and horizontal on-top $c(2\times4)-N_2O/Rh(110)$ structures. An analogous PDOS plot is also shown for the ''noninteracting'' system, where the N_2O is located ~6 Å above the surface. Fermi level is chosen as the zero energy level for these plots. The molecular-derived peaks are labeled by corresponding molecular-orbital symmetries. To help the interpretation of the figure, we plotted the molecular valence

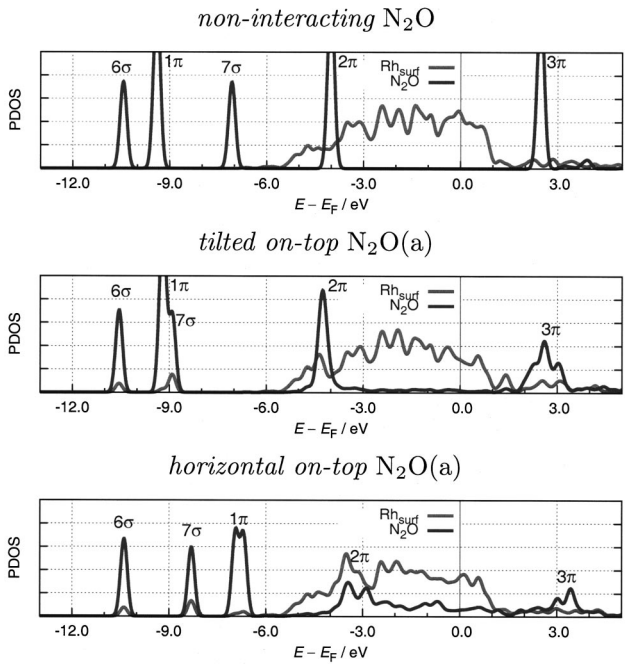

FIG. 6. Density of states projected (PDOS) to the N_2O molecule and to the surface Rh atoms, labeled as Rh_{surf} that interact with the N_2O molecule. The top panel shows the PDOS for the "noninteracting" system (i.e., the N_2O is located ~6 Å above the surface), the middle panel shows the PDOS of the tilted on-top structure, while the bottom panel shows the PDOS for the horizontal on-top $c(2\times4)-N_2O/Rh(110)$ structure. The characters of the derived molecular peaks of N_2O are also shown (labeling of the molecular states refer to the gas phase N_2O). Fermi level is chosen as the zero energy level for these plots and is indicated by a vertical solid line. The PDOSs are Gaussian broadened with a broadening parameter of 0.15 eV.

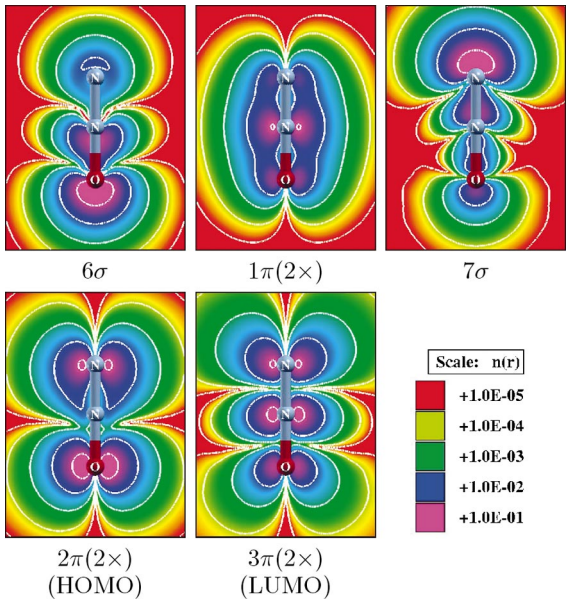

FIG. 7. (Color) Plots of calculated square modulus of valence and LUMO molecular orbitals of the gas phase N_2O molecule $|\phi_i(\mathbf{r})|^2$. Contours are drawn in a logarithmic scale (five contours from $10^{-5}e/a_0^3$ to $10^{-1}e/a_0^3$) and plots are colored rainbowlike (the magnitude of the plotted orbitals increases from red to violet).

and LUMO (lowest-unoccupied-molecular-orbital) states of the isolated molecule in Fig. 7, while the visualization of molecular states of the interacting molecule is utilized by the ILDOS plots shown in Fig. 8. The valence molecular 4σ and 5σ states lie more than 10 eV below the 6σ state and are not shown in Figs. 6, 7, and 8. By comparison of the two PDOS plots of interacting structures with that of the noninteracting one, we see that the PDOS of the tilted structure is affected far less by adsorption than the PDOS of the horizontal form. Although the symmetry of the horizontal N_2O is reduced from $C_{\infty v}$ to C_S, and the π orbitals are split into corresponding a' and a'' states, we will still refer—for the ease of discussion—to the σ and π orbital notation of linear N_2O. The only noticeable differences of the PDOS of the tilted structure compared to the noninteracting structure is a significant downshift of 7σ molecular orbital and broadening of the 3π LUMO state. For the horizontal on-top structure the 7σ orbital is also downshifted. The 1π orbitals are slightly split (see a double peak) and upshifted so significantly that the change in the relative order of the 1π and 7σ states occurs. The 2π (i.e., $9a'$ and $2a''$) and 3π (i.e., $10a'$ and $3a''$) states are substantially broadened. There is a significant contribution of the molecular states in between the 2π HOMO (highest-occupied-molecular-orbital) and 3π LUMO peaks. As revealed by the ILDOS plots depicted in Fig. 8, this contribution is composed of molecular states of the 2π and 3π character that are coupled with the substrate d states (see ILDOS plot labeled as $2\pi+3\pi$). The 3π spill all the way down to the 2π peak, as can be recognized from the ILDOS plot for the 2π energy window. The 3π-related features present below the Fermi level are a clear indication of the substrate charge backdonation into the molecular 3π LUMO level.

Now we compare the tilted O-bonded form with the horizontal $N_2O(a)$ form. It is interesting that the O-tilted form is not able to form a bond with the surface, while the O atom interacts readily with the surface in the horizontal form. The latter is demonstrated by the $\Delta n(\mathbf{r})$ plot of Fig. 5, the ILDOS plot of Fig. 8, and the PDOS plots shown in Fig. 9 where the molecular PDOS is decomposed into the PDOS projected to N_t and O atoms. There is significant contribution of O-projected density of states (DOS), starting near the bottom of the substrate d bands and continuing to the Fermi level—an indication of "through oxygen" N_2O-surface interaction. In fact, the coupling of the molecular π states with the metal d states is more pronounced in the DOS projected to O than to N_t atom. Despite that, the O-surface interaction is effective only for the horizontal form and not for the tilted O-bonded form.

V. CONCLUSIONS

The adsorption structures of N_2O on Rh(110) predicted by DFT within the GGA approximation have been characterized in detail. As the main result two stable forms of $N_2O(a)$ were found. The first, less stable form is tilted with the terminal N atom attached to the surface, while the second, more stable form lies horizontally on the surface. Adsorption on the on-top site is preferable for both forms. The tilted form remains linear on adsorption with the intramolecular distances almost unchanged. On the other hand, the horizontal form is bent, with the terminal-nitrogen and oxygen atoms

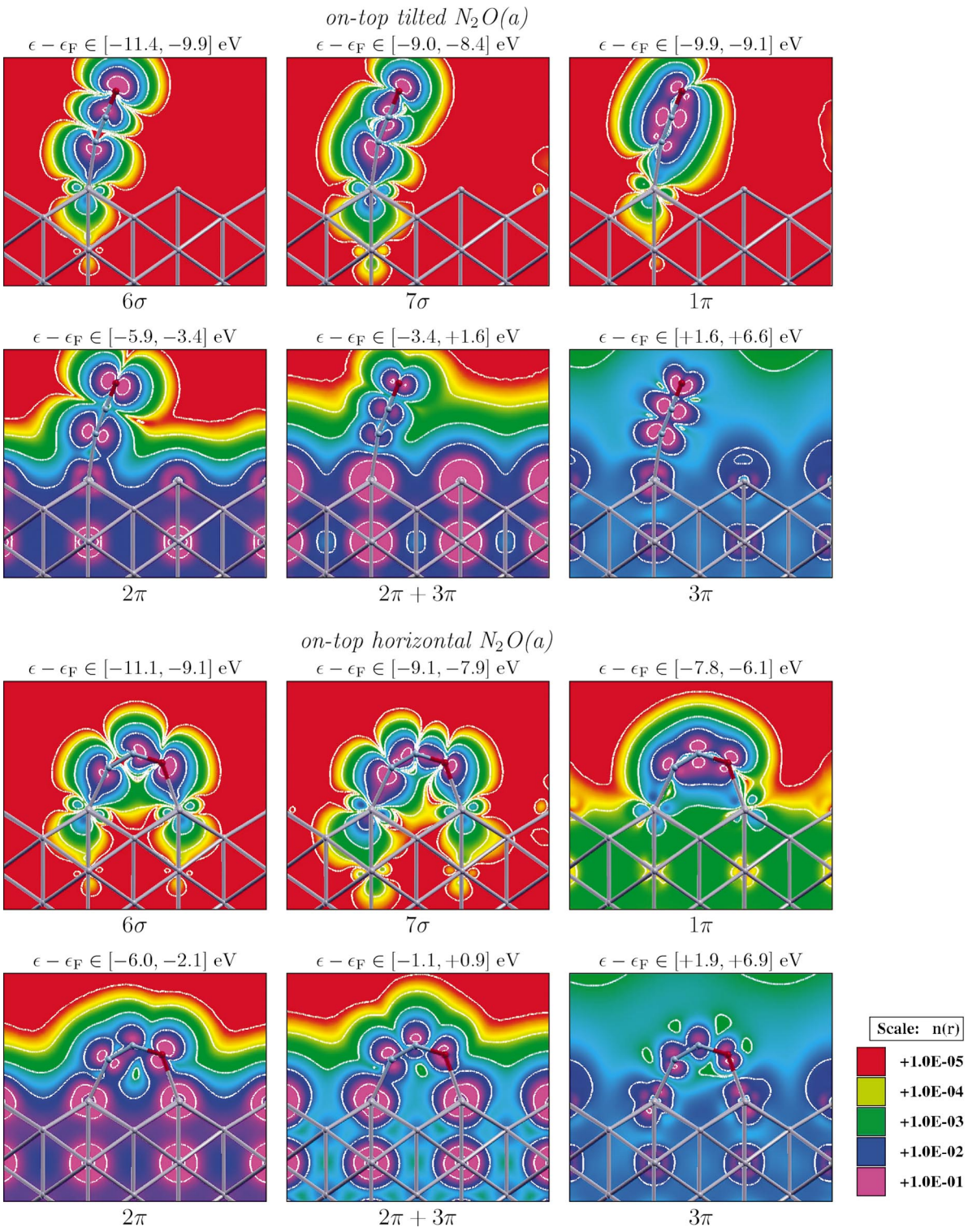

FIG. 8. (Color) Contour plots of integrated local density of states (ILDOS) for the on-top tilted and horizontal c(2×4)−N_2O/Rh(110) structures. Five contours are drawn in logarithmic scale from $10^{-1}e/a_0^3$ to $10^{-5}e/a_0^3$. The magnitude of the plotted increases from red to violet in rainbow fashion. Each shown ILDOS is associated with a given energy window—Fermi level is chosen as the zero energy—as written above each plot (refer to corresponding PDOS plots of Fig. 6).

pointing towards the surface. The intramolecular distances are greater than in the tilted form due to larger charge back-donation into the antibonding 3π molecular orbital as evidenced by the electronic structure analysis.

At high coverage $\Theta \sim 1$ ML the adjacent tilted molecules point in opposite direction, i.e., out-of-phase tilting configuration, while already at 1/2 ML coverage the difference in binding energy between the out-of-phase and in-phase tilting configurations is insignificant.

An interesting result is that at lower adsorbate coverage $\Theta \lesssim 1/4$ ML the adsorption of some horizontal N_2O forms is dissociative, i.e., $N_2O \rightarrow N_2(a) + O(a)$. This is presumably

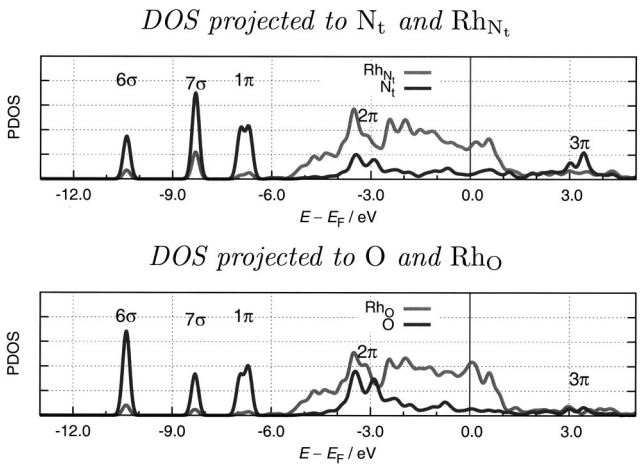

FIG. 9. PDOS for the on-top horizontal $c(2\times4)-N_2O/Rh(110)$ structure. Top panel shows projection to the N_t and the Rh atom located beneath the N_t atom, labeled as Rh_{N_t}, while in bottom panel, projection onto the O and the Rh atom located beneath the O atom, labeled as Rh_o, are shown. Fermi level is chosen as the zero energy level for these plots and is indicated by a vertical solid line. The PDOSs are Gaussian-broadened with a broadening parameter of 0.15 eV.

due to the absence of dissociation barrier or at least very narrow and small dissociation barrier.

The undissociated horizontal form is preferentially oriented along the [001] direction and thus bridging atomic troughs of the surface extending in the $[1\bar{1}0]$ direction. However, calculations indicate that also this $N_2O(a)$ form is prone to dissociate, namely, the corresponding dissociation barrier is rather small ~0.15 eV at 1/2 ML coverage and is expected to be even smaller at lower coverage. Therefore further calculations are required to address (i) the stability and dissociation of the horizontal $N_2O(a)$ forms, (ii) the effect of coadsorbed $O(a)$ that is released during the decomposition of N_2O, and (iii) to provide a mechanistic insight into the peculiar inclined N_2 desorption observed experimentally during the thermal dissociation of N_2O.[58,59]

ACKNOWLEDGMENTS

The authors thank Professor Ivan Kobal, Hideyuki Horino, and Dr. Izabela Rzeźnicka for helpful discussions and careful reading of the manuscript. This work was supported financially by the Ministry of Education, Science and Sport of Slovenia, Grant Nos. P2-0148 and P0-0544-0106. A.K. is grateful to Japan Society for the Promotion of Science for financing his research visits to Catalysis Research Center in Sapporo, Japan.

[1] V. I. Pârvulescu, P. Grange, and B. Delmon, Catal. Today **46**, 233 (1998).
[2] M. Shelef and R. W. McCabe, Catal. Today **62**, 35 (2000).
[3] Y. Ohno, K. Kimura, M. Bi, and T. Matsushima, J. Chem. Phys. **110**, 8221 (1999).
[4] Y. Ohno, I. Kobal, H. Horino, I. Rzeźnicka, and T. Matsushima, Appl. Surf. Sci. **169–170**, 273 (2001).
[5] I. Kobal, K. Kimura, Y. Ohno, and T. Matsushima, Surf. Sci. **445**, 472 (2000).
[6] I. Kobal, K. Kimura, Y. Ohno, H. Horino, I. Rzeźnicka, and T. Matsushima, Stud. Surf. Sci. Catal. **130**, 1337 (2000).
[7] H. Horino, S. Liu, A. Hiratsuka, Y. Ohno, and T. Matsushima, Chem. Phys. Lett. **341**, 419 (2001).
[8] H. Horino, S. Liu, M. Sano, S. Wako, A. Hiratsuka, Y. Ohno, I. Kobal, and T. Matsushima, Top. Catal. **18**, 21 (2002).
[9] I. Kobal, A. Kokalj, H. Horino, Y. Ohno, and T. Matsushima, Trends Chem. Phys. **10**, 139 (2002).
[10] H. Horino, I. Rzeźnicka, A. Kokalj, I. Kobal, Y. Ohno, A. Hiratsuka, and T. Matsushima, J. Vac. Sci. Technol. A **20**, 1592 (2002).
[11] S. Liu, H. Horino, A. Kokalj *et al.*, J. Phys. Chem. B **108**, 3828 (2004).
[12] K. Imamura, H. Horino, I. Rzeźnicka *et al.*, Surf. Sci. **566–568**, 1076 (2004).
[13] H. Horino, I. Rzeźnicka, T. Matsushima, K. Takahashi, and E. Nakamura, *UVSOR Activity Report, 2002* (Institute for Molecular Sciences, Okazaki, Japan, 2003), p. 211.
[14] A. Kokalj, I. Kobal, H. Horino, Y. Ohno, and T. Matsushima, Surf. Sci. **506**, 196 (2002).
[15] A. Kokalj, I. Kobal, and T. Matsushima, J. Phys. Chem. B **107**, 2741 (2003).
[16] A. Kokalj, Surf. Sci. **532–535**, 213 (2003).
[17] H. Orita and N. Itoh, Surf. Sci. **550**, 166 (2004).
[18] A. Stirling, J. Phys. Chem. A **102**, 6565 (1998).
[19] A. Delabie, C. Vinckier, M. Flock, and K. Pierloot, J. Phys. Chem. A **105**, 5479 (2001).
[20] A. Delabie and K. Pierloot, J. Phys. Chem. A **106**, 5679 (2002).
[21] A. L. Yakovlev, G. M. Zhidomirov, and R. A. van Santen, Catal. Lett. **75**, 45 (2001).
[22] R. Burch, S. T. Daniells, and P. Hu, J. Chem. Phys. **117**, 2902 (2002).
[23] A. Bogicevic and K. C. Hass, Surf. Sci. **506**, L237 (2002).
[24] J. P. Perdew, K. Burke, and M. Ernzerhof, Phys. Rev. Lett. **77**, 3865 (1996).
[25] D. Vanderbilt, Phys. Rev. B **41**, 7892 (1990).
[26] Ultrasoft pseudopotentials (US PPs) used in this work were obtained from the following references. US PPs for nitrogen and oxygen are from Ref. 58, while the US PP for rhodium is taken from http://www.pwscf.org/pseudo.htm download page (file: Rh.pbe-rrkjus.UPF).
[27] H. J. Monkhorst and J. D. Pack, Phys. Rev. B **13**, 5188 (1976).
[28] M. Methfessel and A. T. Paxton, Phys. Rev. B **40**, 3616 (1989).
[29] S. Baroni, A. Dal Corso, S. de Gironcoli, and P. Giannozzi, *Pwscf and Phonon: Plane-Wave Pseudo-Potential Codes*, codes available from http://www.pwscf.org/ (2004).
[30] A. Kokalj, J. Mol. Graphics Modell. **17**, 176 (1999), code available from: http://www.xcrysden.org/ (2004).
[31] A. Kokalj, Comput. Mater. Sci. **28**, 155 (2003).
[32] N. Bonini, A. Kokalj, A. Dal Corso, S. de Gironcoli, and S. Baroni, Phys. Rev. B **69**, 195401 (2004).
[33] W. H. Press, S. A. Teukolsky, W. T. Vetterling, and B. P. Flannery, *Numerical Recipes in Fortran: The Art of Scientific Computing*, 2nd ed. (Cambridge University Press, Cambridge, 1992).
[34] *CRC Handbook of Chemistry and Physics*, 74th ed., edited by D. R. Lide (CRC, Boca Raton, Florida, 1993).
[35] W. Nichtl, N. Bickel, L. Hammer, K. Heinz, and K. Müller, Surf. Sci. **188**, L729 (1987).
[36] A. Eichler, J. Hafner, and G. Kresse, J. Phys.: Condens. Matter **8**, 7659 (1996).
[37] F. Bondino, G. Comelli, A. Baraldi *et al.*, J. Chem. Phys. **119**, 12525 (2003).
[38] J. Xie and M. Scheffler, Phys. Rev. B **57**, 4768 (1998).
[39] W. R. Tyson and W. A. Miller, Surf. Sci. **62**, 267 (1977).
[40] E. Walker, J. Ashkenazi, and M. Dacoronga, Phys. Rev. B **24**, 2254 (1981).
[41] J. C. Boettger, Phys. Rev. B **49**, 16798 (1994).
[42] A. Lesar and M. Hodošček, J. Chem. Phys. **109**, 9410 (1998).
[43] This structure is a very narrow and shallow local minimum, namely, starting the optimization calculation with too tilted $N_2O(a)$ results in the horizontal on-top tilted N_2O, while starting the calculations with insufficiently tilted $N_2O(a)$ results in "desorbed" N_2O located far away from the surface.
[44] C. Møller and M. S. Plesset, Phys. Rev. **46**, 618 (1934).
[45] Projected densities of states (PDOS) are calculated using the orthonormalized atomic orbitals, say $\tilde{\phi}(\mathbf{r})$, which are defined as: $\tilde{\phi}_\mu(\mathbf{r}) = \Sigma_\nu S_{\mu\nu}^{-1/2}\phi_\nu(\mathbf{r})$, where $S_{\mu\nu}^{-1/2}$ is the element of the square root inverse of the overlap matrix $\mathbf{S}$ of the atomic orbitals $\phi_i(\mathbf{r})$, whose elements are $S_{\mu\nu}=\langle\phi_\mu|\phi_\nu\rangle$. The charge associated with the atomic orbital μ is then: $Q_\mu=\Sigma_v^{\mathrm{occ}}\Sigma_{\mathbf{k}}|\langle\psi_{v,\mathbf{k}}|\tilde{\phi}_\mu\rangle|^2$. This is so called *Löwdin population* analysis.

The PDOS projected onto a given atom or a group of atoms is then obtained by summing the PDOSs of all atomic orbitals located on these atoms. In the present case—due to the use of ultrasoft pseudopotentials—the PDOS equation contain also an augmentation term; see Ref. 59 for the corresponding full expression.

[46] The integrated local density of states (ILDOS) in a given energy range $[E_{\min},E_{\max}]$ is defined as $N(E_{\min},E_{\max},\mathbf{r})=\int_{E_{\min}}^{E_{\max}} n(\epsilon,\mathbf{r})d\epsilon = \Sigma_v \Sigma_{\mathbf{k}} \int_{E_{\min}}^{E_{\max}} |\psi_{v,\mathbf{k}}(\mathbf{r})|^2 \times \delta(\epsilon-\epsilon_{v,\mathbf{k}})d\epsilon$, where $\psi_{v,\mathbf{k}}(\mathbf{r})$ is the vth Bloch orbital at wave-vector $\mathbf{k}$, and $\epsilon_{v,\mathbf{k}}$ is the corresponding energy eigenvalue. In the present case—due to the use of ultrasoft pseudopotentials—this equation contain also an augmentation term; see Ref. 59 for the corresponding full expression.

[47] A. V. Zeigarnik, Kinet. Catal. **44**, 233 (2003).

[48] T. Matsushima, Surf. Sci. Rep. **52**, 1 (2003).

[49] T. E. Madey, N. R. Avery, A. B. Anton, B. H. Toby, and W. H. Weinberg, J. Vac. Sci. Technol. A **1**, 1220 (1983).

[50] N. R. Avery, Surf. Sci. **131**, 501 (1983).

[51] P. Väterlein, T. Krause, M. Bäßler, R. Fink, E. Umbach, J. Taborski, V. Wüstenhagen, and W. Wurth, Phys. Rev. Lett. **76**, 4749 (1996).

[52] G. Ceballos, H. Wende, K. Baberschke, and D. Arvanitis, Surf. Sci. **482–485**, 15 (2001).

[53] E. Umbach and D. Menzel, Chem. Phys. Lett. **84**, 491 (1981).

[54] S. Haq and A. Hodgson, Surf. Sci. **463**, 1 (2000).

[55] S. Polič, M. Senegačnik, I. Kobal, and M. Zieliński, Pol. J. Chem. **75**, 1729 (2001).

[56] H. Horino, I. Rzeźnicka, T. Matsushima, K. Takahashi, and E. Nakamura, *UVSOR Activity Report 2002* (Institute for Molecular Sciences, Okazaki, Japan, 2003), p. 209.

[57] K. Imamura and T. Matsushima, Catal. Lett. **97**, 197 (2004).

[58] A. Dal Corso, Phys. Rev. B **64**, 235118 (2001).

[59] A. Kokalj, A. Dal Corso, S. de Gironcoli, and S. Baroni, J. Phys. Chem. B **106**, 9839 (2002).